American Mineralogist, Volume 79, pages 497–503, 1994

Melting of pyrope, $Mg_3Al_2Si_3O_{12}$, at 7–16 GPa

J. Zhang*
Department of Earth and Environmental Sciences, The City University of New York, New York 10036, U.S.A.

C. Herzberg
Department of Geological Sciences, Rutgers University, New Brunswick, New Jersey 08903, U.S.A.
and Center for High Pressure Research and Department of Earth and Space Sciences, The State University of New York at Stony Brook, Stony Brook, New York 11794, U.S.A.

Abstract

Melting experiments on pyrope have been performed from 7 to 16 GPa using the multianvil press. The results show that the melting curve of pyrope is unusual relative to those for pyroxene and forsterite because either it is linear in T-P space or it has a break in the slope at around 10 GPa. At 3–10 GPa the melting curve appears to be normal in that it can be calculated from reasonable thermodynamic and elastic parameters using the method of minimizing the Gibbs free energy of melting. However, at pressures >10 GPa, the observed melting temperatures are higher than predicted. This can be explained either by cation disordering in crystalline pyrope or by a stiffening of liquid $Mg_3Al_2Si_3O_{12}$ associated with pressure-induced coordination changes involving Al^{3+}. In either case, pyrope is stabilized relative to liquid, and the slope dT/dP of the melting curve is higher than that for enstatite and forsterite at pressures in excess of 10 GPa. The effect of pressure is, therefore, to increase the thermal stability of pyrope at the expense of olivine and to place garnet on the liquidus for komatiite, peridotite, and chondrite compositions.

Introduction

The liquidus phase for komatite, peridotite, and chondrite compositions changes from olivine to garnet at high pressures (Herzberg, 1983; Takahashi, 1986; Ohtani et al., 1986; Ito and Takahashi, 1987; Herzberg et al., 1990; Zhang and Herzberg, 1993), which increases opportunities for garnet fractionation to occur in nature. Garnet fractionation has been demonstrated to be important in understanding the geochemistry of some komatiites (Herzberg, 1992), and it may have occurred during an early differentiation event in the Earth (Ohtani and Sawamoto, 1987; Herzberg and Gasparik, 1991). The melting temperatures of pyrope, $Mg_3Al_2Si_3O_{12}$, at high pressure are therefore important for understanding the stability of garnet in multicomponent systems.

Early studies have shown that pyrope melts incongruently to liquid + spinel or liquid + aluminous enstatite up to 3.5 GPa (Boyd and England, 1962), and it melts congruently at higher pressures (Boyd and England, 1962; Ohtani et al., 1981; Irifune and Ohtani, 1986). Of particular interest in these studies is the slope of the pyrope melting curve, which was reported to change from about 82 °C/GPa at 3.5 GPa to 0 °C/GPa at pressures above 10 GPa (Irifune and Ohtani, 1986). This differs from the melting curve of forsterite, which maintains a positive slope at all pressures (Ohtani and Kumazawa, 1981; Presnall and Walter, 1993). The effect of pressure inferred from these end-member systems is to increase the stability of olivine at the expense of garnet, just the opposite of what is observed in multicomponent systems. A major objective of this work is to resolve this contradiction by reinvestigating the melting curve of pyrope.

Experimental methods and results

All experiments were carried out using the 2000-t split-sphere multianvil apparatus (USSA-2000) located at Stony Brook. A detailed description of the press, the sample assembly, and the techniques has been given in numerous papers (Gasparik, 1989, 1990; Herzberg et al., 1990; Liebermann and Wang, 1992) and is not repeated here.

Two types of starting material were used. One was crystalline pyrope synthesized from a stoichiometric mixture of MgO, Al_2O_3, and SiO_2 at 5 GPa and 1300 °C for 5 h; optical examination and X-ray diffraction showed that the recovered starting material consisted largely of pyrope but contained minor amounts of unreacted oxides. The second type of starting material was a pyrope-free mixture of oxides, and this was used to examine how the experimental results might be affected by the nature of the starting material.

The starting materials were loaded into Re containers, and assemblies of 10 mm were used. These were then fired at 1000 °C in an Ar atmosphere for 1 h prior to the experiment to expel all H_2O. The time to reach the target temperature was 15–30 min, and experiment durations

* Present address: Center for High Pressure Research, Department of Earth and Space Sciences, The State University of New York at Stony Brook, Stony Brook, New York 11794, U.S.A.

0003–004X/94/0506–0497$02.00

Table 1. Experimental results on the melting of pyrope

P (GPa)	T (°C)	t (min)	Starting materials	Expt. products
7.0	1980	3.5	mixture	Py*, L**
8.0	1980	3.0	mixture	Py
8.0	2010	3.0	mixture	Py, L
8.0	2040	4.0	mixture	Py, L
9.0	2035	3.5	mixture	Py
9.0	2070	4.0	mixture	Py
9.5	2060	4.0	mixture	Py
10.0	2110	3.0	pyrope	Py, L
10.0	2050	3.0	pyrope	Py
11.5	2150	3.0	pyrope	Py
11.5	2190	4.0	mixture	Py
13.0	2100	0.5	pyrope	Py
13.0	2200	1.0	pyrope	Py
13.0	2190	3.0	pyrope	Py
13.0	2300	3.0	pyrope	Py, L
14.5	2280	1.0	pyrope	Py
14.5	2300	5 h	mixture	Py
14.5	2365	4.0	mixture	Py
16.0	2200	3.0	pyrope	Py
16.0	2300	3.0	pyrope	Py
16.0	2380	1.0	pyrope	Py
16.0	2500	3.0	pyrope	Py, L

* Py = pyrope.
** L = liquid quenched to glass + extremely fine-grained (<1 μm) intergrowth of crystalline phases.

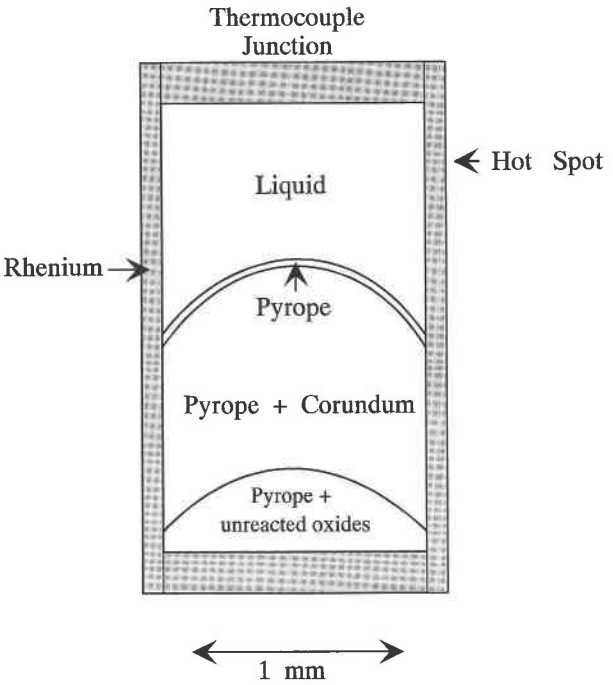

Fig. 1. Sketch of an experiment at 13 GPa and 2300 °C showing the distribution of pyrope, liquid, and unreacted oxides.

at the target temperatures were typically 3 min before the experiments were terminated by shutting off the power. A reversal experiment involving garnet at 2185 °C and 14 GPa demonstrated that equilibrium was reached within 3 min in the presence of a melt phase (Herzberg et al., 1990). The experiment products were prepared as thin sections for optical examination and electron probe analysis (Table 1).

The temperatures given in Table 1 are those recorded by the thermocouple, which was located 0.5 ± 0.2 mm from the hot spot (Fig. 1) and which reads 50 °C lower than the hot-spot temperature of 1200 °C (Gasparik, 1989). The temperature gradient varies as a function of distance along the heater, being flat near the hot spot and steep at the cold end, and is approximately symmetrical on each side of the hot spot. The temperature difference between the hot spot and the cold end of the capsule is 200 °C in the range 1400–1700 °C (Gasparik, 1989) and about 300 °C in the range 2000–2200 °C (Presnall and Gasparik, 1990). In those experiments for which a quench liquid phase is reported in Table 1, the interface with crystalline pyrope is sharp (Fig. 1). The temperature of this interface is the melting temperature of pyrope, and its disposition in all experiments is within 0.7 mm of the hot spot; this results in a thermocouple temperature that is very similar to the melting temperature of pyrope.

Precision in the measurement of temperature is typically ±30 °C (Gasparik, 1990; Presnall and Gasparik, 1990). Temperature accuracy is more problematical because the effect of pressure on thermocouple emf has not been determined and is not included in Table 1. However, it has been estimated to be about −5 °C/GPa (Zhang and Herzberg, 1993), on the basis of the melting temperature of $MgSiO_3$ perovskite determined by a diamond cell heated by a CO_2 laser (2727 ± 50 °C at 22 GPa: Zerr and Boehler, 1993), compared with a multianvil estimation (2600 °C and 22.5 GPa: Gasparik, 1990). If this pressure effect on thermocouple emf is realistic, then the temperatures given in Table 1 are too low by 35 °C at 7 GPa and by 80 °C at 16 GPa. Uncertainties stemming from precision and accuracy should therefore be within ±50 °C.

Irifune and Ohtani (1986) reported that the liquid phase quenches to glass and aluminous enstatite at pressures less than about 7 GPa, and to garnet at higher pressures. The liquid phase in the experiments reported here quenched to an extremely fine intergrowth of glass and quench crystalline phases that were too small to identify by electron probe analysis. In experiments like these, the liquid phase is separated from crystalline pyrope down the temperature gradient by an interface that is invariably sharp (Fig. 1). Pyrope grows with two kinds of morphology, depending on the distance away from the liquid. Within a narrow band 50–100 μm in width next to the liquid (Fig. 1), which translates to about 20 °C down the temperature gradient, the pyrope crystals are the largest in size (10–20 μm), euhedral, and inclusion free. Farther down the temperature gradient, the pyrope crystals are smaller and contain inclusions of corundum. Inclusions of unreacted oxides of SiO_2, Al_2O_3, and MgO occupy the coldest portions of all experimental samples for both types of starting material, crystalline pyrope and mixed oxides, but are completely absent where a liquid phase existed (Fig. 1). Only those parts of the samples that contain in-

clusion-free pyrope bands next to liquid can be considered as stable because a liquid phase is invariably required as a fluxing agent for equilibrium to occur (Gasparik, 1989).

The experimental results listed in Table 1 are shown in Figure 2. Pyrope is interpreted to melt congruently between 7 and 16 GPa, and this is consistent with previous studies between 3.5 and 10 GPa (Boyd and England, 1962; Irifune and Ohtani, 1986). There are many observations in support of this conclusion. Pyrope is the only crystalline phase that is found together with liquid, and the two phases are separated by a very sharp interface (Fig. 1). Electron microprobe analyses of inclusion-free pyrope crystals and rastor microbeam analyses of the adjacent liquid yielded stoichiometric pyrope within analytical error. No other components, including Re from the container, are contained in pyrope. The bands, 10–20 μm in width, of inclusion-free pyrope next to liquid are not an artifact of incongruent melting, but rather they are most reasonably interpreted as arising from the crystallization and melting that occurred from a temperature fluctuation of about ± 10 °C, which is typical of multianvil experiments in the 2000 °C range.

Although we have not explored in detail the effect of starting material preparation on the experimental results by conducting duplicate T-P experiments on both the mixed oxides and the crystalline pyrope, the melting curve shown in Figure 2 describes the results for both starting materials equally well. Similarly, our experimental results at 7–8 GPa using mixed oxides as a starting material are in excellent agreement with the results of Irifune and Ohtani (1986), who used crystalline pyrope. The major difference is in the abundance of mixed oxides that are preserved. In experiments using mixed oxides, large and inclusion-free pyrope crystals invariably grow in bands 50–100 μm wide adjacent to liquid, but the crystals contain a much greater abundance of unreacted oxides in the melt-free cold parts of the charges.

Shown in Figure 2 are out melting temperatures compared with those reported by Irifune and Ohtani (1986). At 7 and 8 GPa there is excellent agreement, but at 9 and 10 GPa our melting temperatures are about 50 °C higher. This difference may be due to ambiguities arising from the rapid transformation of the graphite heaters to diamond in the experiments reported by Irifune and Ohtani (1986) above at 2000 °C and 9–10 GPa. At pressures above 10 GPa, our melting temperatures are 100–350 °C higher than the Kraut-Kennedy extrapolated curve of Irifune and Ohtani (1986). But this extrapolated curve is problematical because it is heavily weighted by their ambiguous measurements at 9–10 GPa.

Discussion

The simplest way of describing the experimental data is with a melting curve that is actually linear in T-P space, and this is shown in Figure 2. The experimental data can be described by:

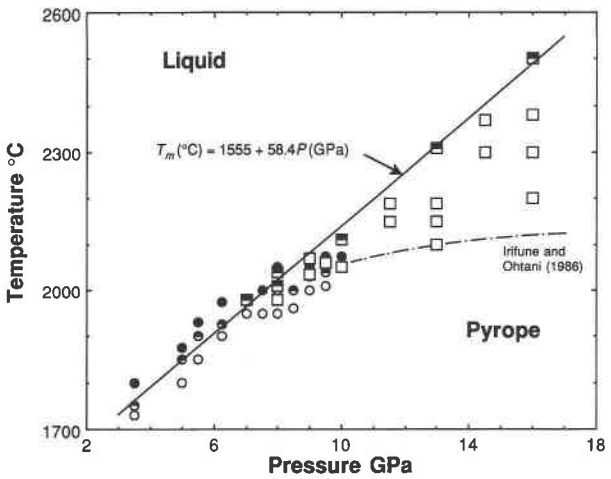

Fig. 2. The experimental results and a linear melting curve for pyrope. Circles = Irifune and Ohtani (1986); squares = this study. Open symbols = solid; solid symbols = quench liquid. The dash-dotted curve is the data of Irifune and Ohtani (1986) fitted by them to a Kraut-Kennedy equation.

$$T_m\ (°C) = 1555 + 58.4P\ (GPa) \quad (1)$$

to within ± 40 °C, which is about the magnitude of the error in the measurement of temperature. But from a thermodynamic point of view, a fusion curve that is linear is difficult to understand because melting involves important changes in volume, and this is usually manifest in melting curves that are indeed curved in T-P space. An attempt was made to model the melting of pyrope by minimizing the Gibbs free energy of melting (Fei et al., 1990), and the results are shown in Figures 3 and 4. Although the data are not of sufficient accuracy to determine whether the melting of pyrope is linear or curved, the calculations that follow are useful for the purpose of developing an understanding of our experimental observations.

The Gibbs free energy of melting has been minimized using standard thermodynamic equations for Gibbs energy, enthalpy, and entropy (e.g., Fei et al., 1990). The heat capacity in these equations, given by $C_P = a + bT + c/T^2 + e/T^3 + g/T$ (e.g., Fei et al., 1990), and the coefficients in Table 2 are a description of calorimetric measurements (Téqui et al., 1991; Richet and Bottinga, 1984). The volume change of melting [i.e., $\Delta V(T,P)$] has been calculated using a third-order Birch-Murnaghan equation of state with several modifications. Although it is common to treat the bulk modulus (K_T) as a linear function of temperature [e.g., $K_T = K_{298} + dK/dT(T - 298)$: Fei et al., 1990], we used $K_T = 1/(\beta_0 + \beta_1 T + \beta_2 T^2 + \beta_3 T^3)$, where β_i are the coefficients of compressibility. This results in better internal consistency among heat capacity, thermal expansion, and the bulk modulus for data systemization with the thermodynamic constraint $C_P = C_V + \alpha^2 K_T V T$ (Saxena, 1988; Saxena and Zhang, 1989; Saxena and Shen, 1992). The term $V(1,298)/V(P,298)$ in

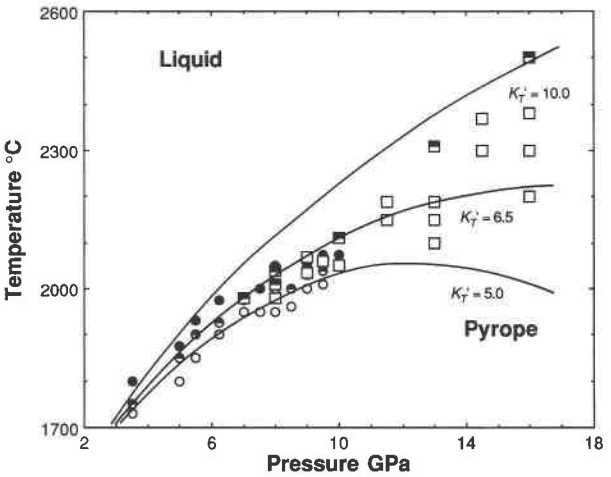

Fig. 3. The experimental results and calculated melting curves for pyrope. Melting curves were calculated for completely ordered pyrope using the thermodynamic and elastic parameters listed in Table 2. The three melting curves show how changes in the pressure derivative of the bulk modulus K_T' for the liquid can affect the results. Note that higher values of K_T' stabilize pyrope relative to liquid. The symbols are as for Fig. 2.

TABLE 2. Thermodynamic properties of $Mg_3Al_2Si_3O_{12}$ pyrope and liquid

Parameters	Pyrope	Liquid
ΔH°_{1570} (J/mol)	−5697713	−5456713
ΔS°_{1570} [J/(mol·K)]	1005.5	1159.6
Heat capacity C_P [J/(mol·K)] = $a + bT + c/T^2 + e/T^3 + g/T$		
a	519.70	630.00
b	0.0139	0.035
c (× 10^7)	−0.5161	—
e (× 10^5)	−0.5074	—
g (× 10^5)	−0.4194	—
V_{298} (cm/mol)	113.37	136.50
α (K^{-1}) = $\alpha_0 + \alpha_1 T + \alpha_2/T^2$		
α_0 (10^{-4})	0.2428	0.565
α_1 (10^{-8})	0.2578	—
α_2	−0.4421	—
K_T (GPa) = $1/\beta$; $\beta = (\beta_0 + \beta_1 T + \beta_2 T^2 + \beta_3 T^3)$		
β_0 (10^{-6})	0.5501	5.4054
β_1 (10^{-10})	0.8643	—
β_2 (10^{-14})	0.4798	—
β_3 (10^{-18})	0.1398	—
K_T'	4.93	6.5 (3–10 GPa)

Note: pyrope: ΔH°_{1570}, Charlu et al. (1975) and Téqui et al. (1991); ΔS°_{1570}, Haselton and Westrum (1980) and Téqui et al. (1991); C_P, Téqui et al. (1991); V_{298}, Robie et al. (1978); α, Skinner (1966); β, O'Neill et al. (1991); K_T', Webb (1989). Liquid: ΔH°_{1570} and ΔS°_{1570}, Téqui et al. (1991); C_P, Richet and Bottinga (1984); α and β, Lange and Carmichael (1987); V_{298} and K_T', this study; ΔH°_{1570} and ΔS°_{1570} = the standard enthalpy and entropy at 1570 K; C_P = heat capacity; V°_{298} = molar volume at 298 K; α = thermal expansion; K_T and β = isothermal bulk modulus and compressibility, respectively; K_T' = pressure derivative of the bulk modulus.

the original Birch-Murnaghan equation has been replaced by $V(1,T)/V(P,T)$, where

$$V(1,T) = V_{298}\left[\exp\left(\int_{298}^{T} \alpha \, dT\right)\right].$$

V_{298} is the molar volume at 298.15 K and 1 atm, and α is the coefficient of isobaric thermal expansion as given by $\alpha = \alpha_0 + \alpha_1 T + \alpha_2/T^2$. Heat capacity, thermal expansion, and bulk modulus data are listed in Table 2. The high-temperature bulk modulus of pyrope calculated from the $C_P - C_V$ relation is in good agreement with the data of Anderson et al. (1991) within the temperature range of their measurements.

The molar volume of $Mg_3Al_2Si_3O_{12}$ liquid from Lange and Carmichael (1987) yields a calculated melting curve for pyrope that is 100–250 °C higher than what we observe in the range 3–10 GPa. A more successful simulation is obtained with a molar volume that is 3.4% lower (Table 2), and the results are shown in Figure 3. At pressures <10 GPa, we calculate a melting curve that is in excellent agreement with our experimental data for the following $Mg_3Al_2Si_3O_{12}$ liquid parameters: $V^\circ_{298} = 136.5 \pm 4.0$ cm³/mol, $K_T = 18.5 \pm 1.0$ GPa, and $K_T' = 6.5 \pm 1.5$, where V°_{298} is the molar volume at 298 K, K_T is the isothermal bulk modulus, and K_T' is the pressure derivative of the bulk modulus. The errors associated with these estimates are based on errors reported for the entropy and enthalpy of melting (Téqui et al., 1991), uncertainties in temperature (above), and uncertainties in the molar volume of crystalline pyrope (Skinner, 1956). But at pressures >10 GPa, our preferred volume parameters yield melting temperatures that are too low. By increasing K_T' from 6.5 to 10, it is possible to calculate a melting temperature at 16 GPa that matches our experimental observations, but it yields melting temperatures that are too high in the range 3–10 GPa (Fig. 3). We cannot produce a melting curve from a single set of elastic constants that fits the entire data base in the range 3–16 GPa.

Another possible way of describing the melting curve is shown in Figure 4. It has a slope that gradually decreases from 82 °C/GPa at 3.5 GPa to 35 °C/GPa at 9–10 GPa (Boyd and England, 1962; Irifune and Ohtani, 1986); at pressures above 10 GPa, our data require a slope that is about 65 °C/GPa, indicating the possible existence of a breaking in the slope of the melting curve. The increased stabilization of pyrope relative to liquid in the range 10–16 GPa indicates the occurrence of structural changes in either pyrope or liquid. The most obvious possibility is a phase transformation in crystalline pyrope. To test this idea, a synthesis experiment was conducted at 14.5 GPa and 2200 °C for 5 h. X-ray diffraction of the recovered sample yielded a standard JCPDS pyrope pattern, with minor peaks attributed to unreacted corundum, indicating that the garnet is somewhat deficient in Al_2O_3. As discussed above, equilibrium was probably not reached because of the absence of a liquid phase in this experiment. However, the results suggest that no phase transformation occurred in crystalline pyropic garnet, unless it is fundamentally nonquenchable in nature.

If cation disordering occurred in the crystallographic sites of pyrope, the configurational entropy would lower its Gibbs energy, pyrope would become stabilized relative to liquid, and this could change the T-P slope of the melting curve. In addition, some disordering in pyrope may be anticipated because disordering of Mg and Si has been

observed in the octahedral sites in $MgSiO_3$ majorite garnet synthesized at 2000 °C (Phillips et al., 1992). From the thermodynamic parameters in Table 2, we calculate that only 9.8 and 21.3 J/(mol·K) are needed to raise the melting temperatures from a completely ordered pyrope melting curve (see Fig. 3; $K'_T = 6.5$) to temperatures we determined at 13 and 16 GPa, respectively.

Pyrope, with a structural formula $^{[8]}Mg_3{}^{[6]}Al_2{}^{[4]}Si_3O_{12}$, has Si in tetrahedral sites, Al in octahedral sites, and Mg in dodecahedral sites in its completely ordered state. The spectroscopic studies of McMillan et al. (1989) on pyrope synthesized at 900–1000 °C showed no disordering, but the site occupancies of interest here are those above 2100 °C. The configurational entropy of cation disordering is calculated from the relation $S_c = -nR[\Sigma X_j^i \ln X_j^i]$, where n is the number of j sites per formula unit, R is the gas constant, and X_j^i the cation site occupancy of an i atom (i = Mg, Al, Si) on a j crystallographic site (j = the dodecahedral site preferred by Mg, the octahedral site preferred by Al, and the tetrahedral site preferred by Si). As no crystallographic or spectroscopic information on high-temperature pyrope exists, we consider a few possible cases. For the total mixing of Al and Si in two octahedral sites and three tetrahedral sites, the configurational entropy is 28 J/(mol·K). In the unlikely event that Al should mix with Mg in the unusual dodecahedral site, the total mixing of Mg and Al in three dodecahedral sites and two octahedral sites is also 28 J/(mol·K). The maximum possible configurational entropy is 37.4 J/(mol·K) from the mixing of Mg and Al in three dodecahedral sites and one octahedral site, in addition to the mixing of Al and Si in one octahedral site and three tetrahedral sites. Whatever the case may be, these configurational entropy values are significantly higher than the 9.8 and 21.3 J/(mol·K) of extra entropy that are needed to raise the melting temperature of ordered pyrope to the temperatures that we experimentally observed at 13 and 16 GPa, respectively, indicating that disorder may be partial and temperature dependent. Another source of extra entropy in pyrope is from positional disorder of the small Mg cation at high temperatures if thermal expansion is accommodated by a substantial increase in the size of the large dodecahedral site. In any case, it is concluded that cation disordering in pyrope at temperatures above 2100 °C is a possible way of explaining our experimental data and may explain why the melting curve has the break in slope at 10 GPa (Fig. 4).

We conclude this analysis with an examination of possible changes in the properties of pyrope liquid. The most obvious consideration involves possible Al^{3+} coordination changes in the liquid from fourfold to sixfold coordination at around 10 GPa, where there may be a break in the melting slope. The evidence for coordination increases in Al^{3+} at about this pressure was from ^{27}Al solid-state NMR measurements on silicate glasses (Ohtani et al., 1985; Xue et al., 1991), molecular dynamics simulations (Angell et al., 1982, 1987), and the observation of garnet quenched from liquid pyrope at pressures >7 GPa (Irifune and Ohtani, 1986). The essential question involves how these structural changes affect the volume of pyrope liquid.

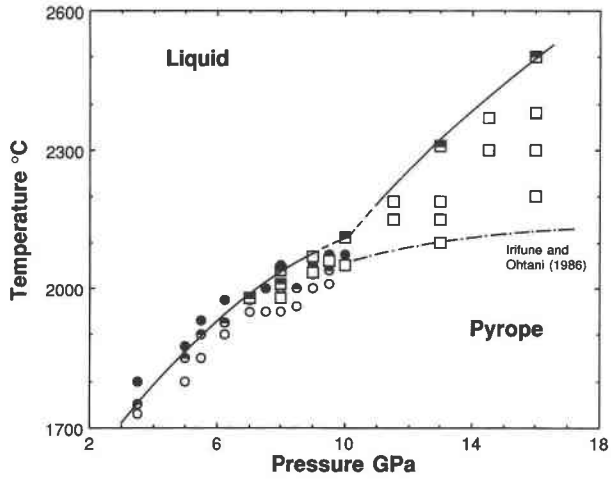

Fig. 4. The experimental results and a melting curve for pyrope. The curve from 3 to 10 GPa was calculated with a pressure derivative of the bulk modulus $K'_T = 6.5$, from Fig. 3. At 10–16 GPa the curve is empirical. The dash-dotted curve is the data of Irifune and Ohtani (1986) fitted by them to a Kraut-Kennedy equation. The broken curve indicates the pressure range where a break in the melting curve is possible. The symbols are as for Fig. 2.

For pyrope that is assumed to remain fully ordered at all conditions, the only way that melting temperatures can be raised is by increasing K'_T for $Mg_3Al_2Si_3O_{12}$ liquid from 6.5 at $P < 10$ GPa to about 10 at 16 GPa, as indicated in Figure 3. The effect this has on the molar volume of $Mg_3Al_2Si_3O_{12}$ liquid is shown in Figure 5 and is calculated from the melting curve (Fig. 4) using thermochemical parameters for a fully ordered pyrope (Table 2). It is demonstrated that there is a tendency for $Mg_3Al_2Si_3O_{12}$ liquid to stiffen at >10 GPa and 2000 °C, an arbitrarily selected temperature. Rigden et al. (1988) also observed this kind of behavior from shock-wave experiments on molten $An_{0.36}Di_{0.64}$, a composition that contains 15.4% Al_2O_3. The volume in their experiments was observed to change gradually over the pressure interval from 1 atm to 25 GPa, but negligibly at higher pressures. Rigden et al. (1988) interpreted their results to indicate a gradual transformation of Al and Si from dominantly tetrahedral to octahedral coordination in the range 1 atm to 25 GPa; at higher pressures they suggested that these transformations may be essentially complete, and there may be a similarity in the compressibilities of the liquid and an increase in the melting slope of $MgSiO_3$ perovskite at around 60 GPa, but this break has not been verified by Zerr and Boehler (1993). This interpretation, however, is ambiguous because P-V breaks were not observed in shock-wave experiments for molten anorthite (36.6% Al_2O_3: Rigden et al., 1989) and for molten komatiite (8.2% Al_2O_3: Miller et al., 1991) over a comparable pressure range. Furthermore, the melting curve of jadeite ($NaAlSi_2O_6$) from 2.4 to 16.5 GPa shows no T-P breaks (Fig.

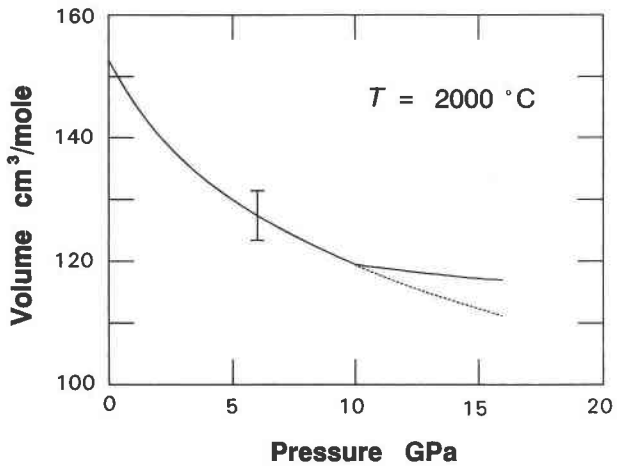

Fig. 5. Possible P-V relations of liquid $Mg_3Al_2Si_3O_{12}$ at 2000 °C derived from the melting of ordered pyrope along the melting curve in Fig. 4. The solid curve was calculated from the elastic and thermodynamic parameters listed in Table 2, with K'_T raised from 6.5 to 10.2 at pressures in the range 10–16 GPa. The broken curve was calculated with $K'_T = 6.5$ (Fig. 3). Errors stemming from uncertainties in temperature, enthalpy, and entropy of melting and from the molar volume of crystalline pyrope are ±4 cm³/mol.

6) that could be attributed to structural changes that are known to occur in albite glass (Ohtani et al., 1985). The evidence is therefore somewhat contradictory, but the bulk of it indicates that disordering in pyrope may be more important than structural changes in liquid $Mg_3Al_2Si_3O_{12}$. Spectroscopic studies on pyrope synthesized at around 2500 °C could be important in constraining these possibilities.

Figure 6 summarizes the melting curve of pyrope in relation to the melting curves of enstatite (Boyd et al., 1964; Presnall and Gasparik, 1990), forsterite (Davis and England, 1964; Ohtani and Kumazawa, 1981; Presnall and Walter, 1993), and jadeite (Litvin and Gasparik, 1993). The very high melting temperatures observed for pyrope at around 15 GPa show that pressure stabilizes garnet at the expense of forsterite, in agreement with phase equilibrium studies in multicomponent systems (Takahashi, 1986; Ohtani et al., 1986; Ito and Takahashi, 1987; Herzberg et al., 1990; Zhang and Herzberg, 1993). We emphasize that the experimental method utilized in this study is identical to that used for the enstatite and forsterite fusion curves (Presnall and Gasparik, 1990; Herzberg et al., 1990; Presnall and Walter, 1993), and it is also identical to the method used in calibrating the solidus curve in peridotite systems (Herzberg et al., 1990). Therefore, the results presented here cannot be an artifact of the experimental method.

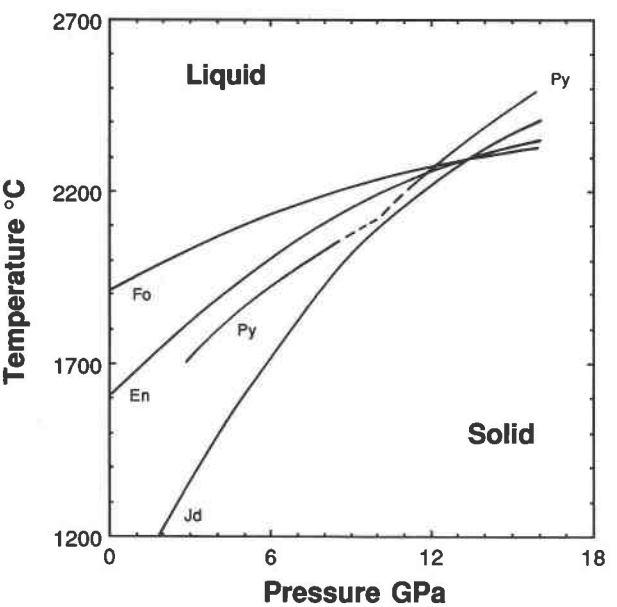

Fig. 6. The melting curve of pyrope compared with those for enstatite (Presnall and Gasparik, 1990), forsterite (Presnall and Walter, 1993), and jadeite (Litvin and Gasparik, 1993).

Acknowledgments

This research was partially supported by grants from the National Science Foundation to Claude Herzberg (EAR-8916836 and EAR-9117184). The high-pressure experiments reported in this paper were performed in the Stony Brook High Pressure Laboratory, which is jointly supported by the National Science Foundation (EAR-8917563) and the State University of New York at Stony Brook. This laboratory is now a part of the NSF Science and Technology Center for High Pressure Research (EAR-8920239) established at Stony Brook in conjunction with Princeton University and the Geophysical Laboratory of the Carnegie Institution of Washington. Thanks are extended to J. Bass, G. Harlow, G. Miller, E. Ohtani, and L. Stixrude for their helpful discussions and comments. Special thanks are extended to Tibor Gasparik for technical assistance. This is Mineral Physics Institute Publication no. 78.

References cited

Anderson, O.L., Isaak, D.L., and Oda, H. (1991) Thermoelastic parameters for six minerals at high temperature. Journal of Geophysical Research, 96, 18037–18046.

Angell, A.C., Cheesman, P., and Tamaddon, S. (1982) Pressure enhancement of ion mobilities in liquid silicates from computer simulation studies to 800 kilobars. Science, 218, 885–887.

Angell, A.C., Cheesman, P., and Kadiyala, R.R. (1987) Diffusivity and thermodynamic properties of diopside and jadeite by computer simulation studies. Chemical Geology, 62, 83–92.

Boyd, F.R., and England, J.L. (1962) Mantle minerals. Carnegie Institution of Washington Year Book, 61, 107–112.

Boyd, F.R., England, J.L., and Davis, B.T.C. (1964) Effects of melting and polymorphism of enstatite, $MgSiO_3$. Journal of Geophysical Research, 69, 2101–2109.

Charlu, T.V., Newton, R.C., and Kleppa, O.J. (1975) Enthalpies of formation at 970 K of compounds in the system MgO-Al_2O_3-SiO_2 from high temperature solution calorimetry. Geochimica et Cosmochimica Acta, 39, 1487–1497.

Davis, B.T.C., and England, J.L. (1964) The melting of forsterite up to 50 kilobars. Journal of Geophysical Research, 69, 1113–1116.

Fei, Y., Saxena, S.K., and Navrotsky, A. (1990) Internally consistent data and equilibrium phase relations for compounds in the system MgO-SiO_2 at high pressure and high temperature. Journal of Geophysical Research, 95, 6915–6928.

Gasparik, T. (1989) Transformation of enstatite-diopside-jadeite pyroxenes to garnet. Contributions to Mineralogy and Petrology, 102, 389–405.

——— (1990) Phase relations in the transition zone. Journal of Geophysical Research, 95, 15751–15769.

Haselton, H.T., and Westrum, E.F. (1980) Thermodynamics of grossular-pyrope garnets and their stabilities at high temperatures and high pressures. Journal of Geophysical Research, 85, 6973–6982.

Herzberg, C. (1983) Solidus and liquidus temperatures and mineralogies for anhydrous garnet-lherzolite to 15 GPa. Physics of the Earth and Planetary Interiors, 32, 193–202.

——— (1992) Depth and degree of melting of komatiites. Journal of Geophysical Research, 97, 4521–4540.

Herzberg, C., and Gasparik, T. (1991) Garnet and pyroxenes in the mantle: A test of the majorite fractionation hypothesis. Journal of Geophysical Research, 96, 16263–16274.

Herzberg, C., Gasparik, T., and Sawamoto, H. (1990) Origin of mantle peridotite: Constraints from melting experiments up to 16.5 GPa. Journal of Geophysical Research, 95, 15779–15803.

Irifune, T., and Ohtani, E. (1986) Melting of pyrope $Mg_3Al_2Si_3O_{12}$ up to 10 GPa: Possibility of a pressure-induced structural change in pyrope melt. Journal of Geophysical Research, 91, 9357–9366.

Ito, E., and Takahashi, E. (1987) Melting of peridotite under the lower mantle condition. Nature, 328, 514–517.

Knittle, E., and Jeanloz, R. (1989) Melting curve of $(Mg,Fe)SiO_3$ perovskite to 96 GPa, evidence for a structural transition in lower mantle melts. Geophysical Research Letters, 16, 421–424.

Lange, R.A., and Carmichael, I.S.E. (1987) Densities of Na_2O-K_2O-CaO-MgO-FeO-Fe_2O_3-Al_2O_3-TiO_2-SiO_2 liquids: New measurements and derived partial molar properties. Geochimica et Cosmochimica Acta, 51, 2931–2946.

Liebermann, R.C., and Wang, Y. (1992) Characterization of sample environment in a uniaxial split-sphere apparatus. In Y. Syono and M.H. Manghnani, Eds., High-pressure research: Application to Earth and planetary sciences, p. 19–31. Terra Scientific, Tokyo, and American Geophysical Union, Washington, DC.

Litvin, Y.A., and Gasparik, T. (1993) Melting of jadeite to 16.5 GPa and melting relations on the enstatite-jadeite join. Geochimica et Cosmochimica Acta, 57, 2033–2040.

McMillan, P., Akaogi, M., Ohtani, E., Williams, Q., Nieman, R., and Sato, R. (1989) Cation disorder in garnets along the $Mg_3Al_2Si_3O_{12}$-$Mg_4Si_4O_{12}$ join: An infrared, Raman and NMR study. Physics and Chemistry of Minerals, 16, 428–435.

Miller, G.H., Stolper, E.M., and Ahrens, T.J. (1991) The equation of state of a molten komatiite. I. Shock wave compression to 36 GPa. Journal of Geophysical Research, 96, 11831–11848.

Ohtani, E., and Kumazawa, M. (1981) Melting of forsterite Mg_2SiO_4 up to 15 GPa. Physics of the Earth and Planetary Interiors, 27, 32–38.

Ohtani, E., and Sawamoto, H. (1987) Melting experiments on a model chondritic mantle composition at 25 GPa. Geophysical Research Letters, 14, 733–736.

Ohtani, E., Irifune, T., and Fujino, K. (1981) Fusion of pyrope at high pressures and rapid crystal growth from the pyrope melt. Nature, 294, 62–64.

Ohtani, E., Taulelle, F., and Angell, C.A. (1985) Al^{3+} coordination changes in liquid aluminosilicates under pressure. Nature, 314, 78–81.

Ohtani, E., Kato, T., and Sawamoto, H. (1986) Melting of a model chondritic mantle to 20 GPa. Nature, 322, 352–353.

O'Neill, B., Bass, J.D., Rossman, G.R., Geiger, C.A., and Langer, K. (1991) Elastic properties of pyrope. Physics and Chemistry of Minerals, 17, 617–621.

Phillips, B.P., Howell, D.A., Kirkpatrick, R.J., and Gasparik, T. (1992) Investigation of cation order in $MgSiO_3$-rich garnet using ^{29}Si and ^{27}Al MAS NMR spectroscopy. American Mineralogist, 77, 704–712.

Presnall, D.C., and Gasparik, T. (1990) Melting of enstatite from 10 to 16.5 GPa, the beta phase-majorite eutectic at 16.5 GPa, and implications for the origin of the mantle. Journal of Geophysical Research, 95, 15771–15777.

Presnall, D.C., and Walter, M.J. (1993) Melting of forsterite, Mg_2SiO_4, from 9.7 to 16.5 GPa. Journal of Geophysical Research, 98, 19777–19783.

Richet, P., and Bottinga, Y. (1984) Anorthite, andesine, wollastonite, diopside, cordierite, and pyrope: Thermodynamics of melting, glass transitions, and properties of the amorphous phases. Earth and Planetary Science Letters, 67, 415–422.

Rigden, S.M., Ahrens, T.J., and Stolper, E.M. (1988) Shock compression of molten silicate: Results for a model basaltic composition. Journal of Geophysical Research, 93, 367–382.

——— (1989) High-pressure equation of state of molten anorthite and diopside. Journal of Geophysical Research, 94, 9508–9522.

Robie, R.A., Hemingway, B.S., and Fisher, J. (1978) Thermodynamic properties of minerals and related substances at 298.15 K and 1 bar (10^5 Pascals) and at high temperatures. U.S. Geological Survey Bulletin, 1452, 452 p.

Saxena, S.K. (1988) Assessment of thermal expansion, bulk modulus, and heat capacity of enstatite and forsterite. Physics and Chemistry of Solids, 49, 1233–1235.

Saxena, S.K., and Shen, G. (1992) Assessment of thermophysical and thermochemical data in some oxides and silicates. Journal of Geophysical Research, 97, 19813–19825.

Saxena, S.K., and Zhang, J. (1989) Assessed high-temperature thermochemical data on some solids. Physics and Chemistry of Solids, 50, 723–727.

Skinner, B.J. (1956) Physical properties of end-members of the garnet group. American Mineralogist, 41, 428–436.

——— (1966) Thermal expansion. In Geological Society of America Memoir, 97, 75–95.

Takahashi, E. (1986) Melting of a dry peridotite KLB-1 up to 14 GPa: Implications on the origin of peridotitic upper mantle. Journal of Geophysical Research, 91, 9367–9382.

Téqui, C., Robie, R.A., Hemingway, B.S., Neuville, D.R., and Richet, P. (1991) Melting and thermodynamic properties of pyrope $Mg_3Al_2Si_3O_{12}$. Geochimica et Cosmochimica Acta, 55, 1005–1010.

Webb, S.L. (1989) The elasticity of the upper mantle orthosilicates olivine and garnet to 3 GPa. Physics and Chemistry of Minerals, 16, 684–692.

Xue, X., Stebbins, J.F., Kanzaki, M., McMillan, P.F., and Poe, B. (1991) Pressure-induced silicon coordination and tetrahedral structural changes in alkali oxide-silica melts up to 12 GPa: NMR, Raman, and infrared spectroscopy. American Mineralogist, 76, 8–26.

Zerr, A., and Boehler, R. (1993) Melting of $(Mg,Fe)SiO_3$-perovskite to 625 kilobars: Indication of a high melting temperature in the lower mantle. Science, 262, 553–555.

Zhang, J., and Herzberg, C. (1993) Melting experiments on peridotite KLB-1 to 22.5 GPa (abs.). American Geophysical Union Spring Meeting, 74, 345.

MANUSCRIPT RECEIVED MAY 10, 1993
MANUSCRIPT ACCEPTED JANUARY 19, 1994